BULLETIN OF THE POLISH ACADEMY OF SCIENCES
TECHNICAL SCIENCES, Vol. 72(5), 2024, Article number: e151041
DOI: 10.24425/bpasts.2024.151041

Current sensor fault-tolerant control based on modified Luenberger observers for safety-critical vector-controlled induction motor drives

Michal ADAMCZYK and Teresa ORLOWSKA-KOWALSKA*

Wroclaw University of Science and Technology, Department of Electrical Machines, Drives and Measurements, Wrocław, Poland

Abstract. Vector-controlled drives require stator current information for use in current feedback and/or state variable estimators. That is why the detection and compensation of possible current sensor (CS) damage is so important. This article focuses on CS fault-tolerant control (FTC) in induction motor (IM) drive systems. In contrast to solutions known from the literature, two modified Luenberger observers (MLO) were applied, allowing for high-quality estimation of currents used in the detector and fault compensator. In a simple implementation of a detection algorithm based on residuals, an adaptive threshold coefficient was employed, enabling effective detection of various types of faults, regardless of whether the second CS was faulty or intact. The presented solution was evaluated during both motor and regenerative operation, with faults occurring in transient states, unlike solutions known in the literature.

Keywords: induction motor drives; fault-tolerant control; current sensor faults; modified Luenberger observers, fault detection, fault compensation.

NOMENCLATURE

State variables:

$\mathbf{u}_s$	spatial vector of stator voltage
$\mathbf{i}_s$	spatial vector of stator current
$\mathbf{\Psi}_s, \mathbf{\Psi}_r$	spatial vectors of stator and rotor fluxes
t_{em}, t_L	electromagnetic and load torques
ω_m	angular rotor speed
$\omega_{s\psi}$	angular synchronous speed of the rotor flux spatial vector
γ_ψ	angle between rotor flux vector and axis A of the stator winding
I_m	instantaneous current amplitude
r_s, r_r	stator and rotor winding resistances
l_s, l_r, l_m	stator, rotor and main inductances of the induction motor
T_M	mechanical time constant
f_{sN}	nominal frequency

Indexes:

ref	reference value
N	nominal value
A, B, C	indexes of components in phase A,B, C coordinate system
α, β	indexes of components in stationary $\alpha - \beta$ coordinate system
x, y	indexes of components in synchronous x–y coordinate system

Abbreviations:

AC	alternating current
CS	current sensor
DC	direct current
FD	fault detection
FC	fault compensation
FTC	fault-tolerant control
IM	induction motor
DFOC	direct field-oriented control
MRAS	model reference adaptive system

1. INTRODUCTION

AC motors are widely used in modern adjustable speed drive (ASD) systems. Induction motor drives, in particular, constitute a significant group of electricity consumers in the industry. Due to their high efficiency, uncomplicated structure, and operational reliability, they are also more and more often used in transportation systems [1], including trams, where electricity is supplied from the traction network or electric cars powered by batteries. Undoubtedly, the drive systems used in these vehicles should be characterized by a high degree of safety because human health and even life depend on their reliability. For this reason, fault-tolerant FTC, described among others in [2–4], has become very popular recently.

FTC can be divided into two main strategies: hardware and software redundancy. In the first case, it is assumed that the measuring, control, and executive devices will be redundant. Such solutions are often applied to frequency converters [5] and, in some situations, to multiphase motors [6], in which the loss of one phase has a smaller impact on the operation of the

*e-mail: teresa.orlowska-kowalska@pwr.edu.pl

Manuscript submitted 2024-04-09, revised 2024-05-29, initially accepted for publication 2024-06-08, published in September 2024.

system than in the case of three-phase motors. In the case of CS faults in drive systems, current measurement is often used in three phases, so that in the event of a failure of one of the CSs, the third one is used as redundant and, based on two measurements, the missing signal in the third phase is determined [7].

The second strategy, which reduces system costs, assumes software solutions based on mathematical models, including state variable observers. These include speed sensorless systems, which are most often associated with the desire to replace expensive speed sensors with various types of estimators, observers, or MRAS systems, widely analysed in the literature [8, 9]. They are used in systems that are assumed to be speed-sensorless, and as software redundancy in FTC drives, in the event of a speed sensor failure [10–12]. Recently, interest in CS-FTC systems has increased significantly, due to the fact that CS fault is a rather common fault in the IM drive [13, 14].

Currently, the most popular CSs are LEM devices. These are non-invasive sensors that use the Hall effect. As a result, the measured current can be represented by the voltage drop across an appropriately selected output resistor, which is then processed by an analogue-to-digital circuit. Due to their structure, they can be characterized by various failures, such as faults to the magnetic core, Hall plate, electronic system, or shunt resistors. Therefore, six types of faults can be distinguished [15]. Less invasive are measurement offsets, gain errors (resulting from fault to the output resistor or wrong scaling of the current signal), or measurement noise. On the other hand, saturation of the magnetic core, intermittent signal decay, or complete loss of the signal significantly affect the operation of the drive system.

There are some methods of compensation for measurement offsets or gain errors in the known literature [13, 16–19]. The simplest solution is to properly increase or decrease the digital value of the current before starting the drive system when this value should be zero. In the event of a gain error, an appropriate function can be used to amplify the CS output signal [19]. The main advantage of such a solution is that there is no need to use mathematical models, owing to which the method is insensitive to changes in motor parameters. However, the disadvantage of this method is the need to use the measurement with a second healthy CS, so this method is not applicable when all the CSs in the drive are faulty. In the case of more serious CS failures, three strategies are proposed in the literature:

- Based on the current measurement of the DC link of the frequency converter.
- Based on reference values of the stator current in the vector control structure.
- Based on mathematical models.

The method of using an additional CS in the DC link of the frequency converter was first proposed by Williams and Green in the late 1980s [20]. Depending on the combination of logic states of the VSI switches, the current flowing through the CS in the DC link (or the voltage drop across the shunt resistor [21]) represents a specific phase current. Despite the simple concept, this method is not widely used in FTC systems, due to its disadvantages, such as the need to use an additional measuring sensor, problems with current measurement resulting, among others, from dead time in IGBT transistors, or the transient state before the current stabilizes [22–25]. Moreover, current measurement is possible only during the duration of active vectors; therefore, this solution, addressed to low-frequency modulation systems, would require modification of transistor connections [26]. Furthermore, compensation for defective CSs is associated with current ripples [23] or with the limitation of the maximum angular velocity of the drive system [25]. For this reason, this solution is mainly addressed to low-cost systems [22, 25].

To compensate for the loss of the signal from the phase CSs in the IM drive, it is possible to use the reference values of the stator current in the vector-controlled structure and the appropriate transformation of the coordinate system [11, 27]. Depending on the CS that has been faulted, the α axis is classically oriented along the A phase or the B phase by rotating the stationary reference frame (α–β) by 120 degrees [11]. This method does not use an IM mathematical model; therefore, this solution is not sensitive to changes in motor parameters. However, this concept was illustrated by tests carried out only in a steady state and in a situation where only one of the two CSs is defective. In the paper [27], the authors added the voltage decoupling of the control paths in the FOC; therefore, they also obtained better properties of the system during transient states.

The third method for stator current reconstruction in the IM drive, which has been an increasingly popular group of solutions in recent years, is based on mathematical models. The authors in [28] propose the use of three state observers. The research carried out by the authors shows the possibility of detecting one or even two faulty CSs when three are used in ASD. However, it is required to measure at least one phase current. The concept of using a single-state observer with simultaneous rotor resistance estimation was presented in [13]. However, in this case, the tests were performed when at least one CS was healthy. In the work [29] an extension of this concept was proposed, and an adaptive observer was applied that allowed simultaneous estimation of the stator and rotor resistance of the IM, to increase the precision of reconstruction of the stator current and rotor flux. This solution requires a speed measurement and a stator current signal from at least one healthy CS available in the system. The authors in [30, 31], proposed a CS-FTC structure without a speed sensor. In post-fault operation, the speed and current estimation performance is achieved by the sliding mode observer. However, as the authors write, the failure of two CSs requires a switch to the open-loop control structure.

Some research has shown that it is possible to estimate the stator current even if all CSs are faulty, but the measured speed is necessary [32–39]. In [32] the authors present a flux-linkage observer (FLO). The stator current is estimated using the stator, rotor, and the mutual fluxes calculated based on the stator voltages and the angular velocity of the motor. In this research, the authors assumed the angular velocity at a level of about 7% of the rated speed and the load torque at about 55% of its rated value. However, the authors presented the detection and compensation of CS faults in a steady state for only one operating condition. As mentioned by the authors, this method is highly sensitive to changes in IM parameters. It is obvious, as after some simple recalculations of the FLO mathematical model,

one can obtain the classical IM model, which is rather sensitive to parameter changes.

The same mathematical model was used in the next concept of stator current reconstruction based on the so-called virtual current sensor (VCS) presented in [33–35]. Studies show the behavior of vector control of the IM drive in a wide range of changes in angular velocity and load torque in the DFOC [33] and in the DTC-SVM [35] structure. As this method is sensitive to changes in rotor resistance, an additional original estimator of this parameter was proposed in [34] activated in post-fault operation. In [36] the authors propose an open loop observer for stator current estimation; however, this solution is the same as the VCS [33] presented earlier. A similar solution was presented in [12]. The authors proposed a recursive least-squares method for the estimation of observer parameters. However, as the authors write, with at least one faulty CS, the parameter identification stops. This makes the solution very sensitive to changes in the IM parameters. In addition, the identification of the observer parameters is highly dependent on the drive operating point, which calls into question the smooth operation of the CS-FTC system under a post-fault situation under different operating conditions.

Another model-based method of stator current estimation is the use of the classical Luenberger observer (LO) [37–39]. The authors in [37–39] presented the possibility of vector control without healthy CS, which means a current sensorless operation. However, it should be mentioned that in these papers the coefficient value in the LO gain matrix was selected close to 1, resulting in a very small gain factor of the LO and an insignificant influence of the stator current error feedback in the proposed LO. In fact, the effective gain coefficients in this feedback were almost negligible, which in practice means that the estimator used is equivalent to the IM model (open-loop observer – OLO, mathematically identical to the VCS presented in [33–35]). The latter will be discussed in detail in the main part of the paper. Moreover, it should be noted that the authors of [37–39] showed the simulation or experimental result only for CS faults occurring in steady states, for a few operating points, for constant speeds, and for constant load torque. The effectiveness of stator current compensation was not shown in the situation when the CS fault occurs in transients or a regenerating mode of the ASD. Moreover, the authors highlighted in [39] that current estimation errors increase for their LO at different operating points (especially for low speed) in the real drive.

This part of the discussion on the proposed model-based stator current estimation methods can be concluded that FLO [32], VCS [33–35], OLO [36], and classical LO with a gain close to zero [37–39] give the same solution prone to IM parameter uncertainties. As shown in [35], the current estimation error in the post-fault operation with VCS increases significantly in the low-speed region and regenerating mode in the real drive, due to changes in motor parameters.

As can be seen from the above review, no CS-FTC solution in the literature would be characterized by an easy-to-implement algorithm of fault detection and compensation, and with the effectiveness confirmed experimentally also in transient states and in the regenerating mode, which is particularly important for such drives as for electric vehicles.

Thus, the research presented in this article aimed to develop a complete CS-FTC system for an IM drive, based on the modified Luenberger observer (MLO), which would enable the detection and compensation of faults for all stator CSs with good accuracy and robustness to motor parameter changes even in transients, for very low speeds, and in regenerating mode. Such an FTC solution could be used in EV and industrial systems with an increased degree of security. The original elements of the proposed method include:

- Unlike methods that employ an open-loop observer or closed-loop observer with extremally low gain factors, the proposed idea uses two modified Luenberger observers (MLO) with a significant gain factor which facilitates both accurate CS fault detection and excellent stator current reconstruction (fault compensation, FC) and well for single as for both CS faults.
- The modification of the Luenberger observer consists of the usage of the available stator current signal when one of the two CS used in the industrial drive is faulty, which improves the accuracy of the missing current reconstruction.
- Using two MLOs, the IM vector control structure can operate if one of two or even both CS used in the drive system are faulty, in all operating conditions of the drive, including speed and torque changes in motoring and regenerating modes, enabling the safety stop of the drive not just after failure is detected but in the time suitable from the point of view of the industrial drive (e.g. in an electric vehicle).
- In the existing literature, the authors emphasize the sensitivity of current estimators to IM parameters. Furthermore, CS fault detection and compensation were conducted only under steady-state operating conditions for motor operation. The proposed solution has improved the accuracy of stator current estimation compared to the approaches used in the literature. As a result, the detection is precise not only in steady-state but also in transient states, for a wide range of speed variations, during both motoring and regenerating modes. This represents a significant advance in CS-FTC systems.
- Stator current estimation is based on existing DC-link voltage and rotor speed measurements and does not require additional CS in the industrial drive. VSI dead-time compensation is also applied.

The article is divided into five sections. Section 2 introduces the mathematical models of the IM, the classical LO, CS faults, and the description of DFOC structure and VSI dead time compensation. Section 3 presents proposed methods: concept of the modification of the LO, proposed CS-FD, CS-FC, and CS-FTC systems. In the fourth section, the experimental results of the proposed CS-FD and CS-FTC are demonstrated under different operating conditions of the IM drive system, including different low speeds and loads, under motor and regenerating mode, for different types of faults. Since faults are the most difficult to detect during transient states, the research focused on these situations. The article is finished with a brief conclusion and summary of the developed CS-FTC drive performance.

2. MATERIALS AND METHODS

2.1. Mathematical model of the induction motor

A mathematical model of an IM can be developed by applying commonly known simplifications [40]. This model can be expressed by using generalized space vectors in a stationary coordinate system (α–β). Additionally, to facilitate the analysis of the results, relative units [p.u.] were used. The application of the above assumptions allows us to present the mathematical model of an IM using the state equation form:

$$T_N \frac{\mathrm{d}}{\mathrm{d}t}\mathbf{x} = \mathbf{A}\,\mathbf{x} + \mathbf{B}\,\mathbf{u}_s\,, \tag{1}$$

with: $\mathbf{x}$ – state vector, $\mathbf{x} = [\mathbf{i}_s,\ \mathbf{\Psi}_r]$, and $\mathbf{A}$ is the state matrix of the IM:

$$\mathbf{A} = \begin{bmatrix} a_1\mathbf{I} & a_2\mathbf{I} - a_3\omega_m\mathbf{J} \\ a_4\mathbf{I} & a_5\mathbf{I} + \omega_m\mathbf{J} \end{bmatrix}, \tag{2}$$

with:

$$\begin{aligned} a_1 &= -\frac{r_s}{\sigma l_s} - \frac{(1-\sigma)r_r}{\sigma l_r},, \quad a_2 = \frac{l_m r_r}{\sigma l_s l_r^2}\,, \\ a_3 &= \frac{l_m}{\sigma l_s l_r}\,, \quad a_4 = \frac{l_m r_r}{l_r}\,, \quad a_5 = -\frac{r_r}{l_r}\,, \end{aligned} \tag{3}$$

and: $\sigma = (l_s l_r - l_m^2)/(l_s l_r)$, $T_N = 1/(2\pi f_{sN})$, $\mathbf{B}$ is the input matrix:

$$\mathbf{B} = \frac{1}{\sigma l_s}\begin{bmatrix} \mathbf{I} \\ \mathbf{0} \end{bmatrix}, \tag{4}$$

where

$$\mathbf{I} = \begin{bmatrix} 1 & 0 \\ 0 & 1 \end{bmatrix}, \quad \mathbf{J} = \begin{bmatrix} 0 & -1 \\ 1 & 0 \end{bmatrix}. \tag{5}$$

Changes in the angular velocity ω_m of the IM are described using the motion equation:

$$T_M \frac{\mathrm{d}}{\mathrm{d}t}\omega_m = t_{em} - t_L\,, \tag{6}$$

where the electromagnetic torque for the IM is described as follows:

$$\begin{aligned} t_{em} &= \frac{l_m}{l_r}\mathrm{Im}\,(\mathbf{\Psi}_r \times \mathbf{i}_s) \\ &= \frac{l_m}{l_r}\left(\Psi_{r\alpha} i_{s\beta} - \Psi_{r\beta} i_{s\alpha}\right). \end{aligned} \tag{7}$$

2.2. Mathematical model of the Luenberger observer

The LO was proposed for the first time in 1971 [41]. This solution is based on the state equation of IM (1) with additional feedback from the information on the state estimation error:

$$T_N \frac{\mathrm{d}}{\mathrm{d}t}\hat{\mathbf{x}} = \mathbf{A}\hat{\mathbf{x}} + \mathbf{B}\,\mathbf{u}_s + \mathbf{G}\,\mathbf{e}_i\,, \tag{8}$$

where $\mathbf{G}$ is the Luenberger observer gain matrix.

Since the rotor flux is a non-measurable state variable, the estimation error $\mathbf{e}_i$ is based on the difference between measured and estimated stator currents:

$$\mathbf{e}_i = \begin{bmatrix} \hat{i}_{s\alpha} - i_{s\alpha} & \hat{i}_{s\beta} - i_{s\beta} \end{bmatrix}^T. \tag{9}$$

The elements of the gain matrix can be derived using the Lyapunov function for stability analysis [41]. For the IM it takes the following form:

$$\mathbf{G} = \begin{bmatrix} G_{12} \\ G_{34} \end{bmatrix} = \begin{bmatrix} g_1\mathbf{I} + g_2\mathbf{J} \\ g_3\mathbf{I} + g_4\mathbf{J} \end{bmatrix}, \tag{10}$$

with:

$$\begin{cases} g_1 = (k_0 - 1)\,(a_1 + a_5)\,, \\ g_2 = (k_0 - 1)\,\omega_m\,, \\ g_3 = \left(k_0^2 - 1\right)(c a_1 + a_4) - c\,(k_0 - 1)\,(a_1 + a_5)\,, \\ g_4 = -c\,(k_0 - 1)\,\omega_m \end{cases} \tag{11}$$

and $c = \sigma l_s l_r / l_m$.

It should be noted that for $k_0 = 1$, this observer becomes an OLO, as all elements of the gain matrix $\mathbf{G}$ (10) go to zero values. Therefore, LO (8) reduces to the state equation of IM (1). The same situation occurs when k_0 is close to zero. Such a solution was used in [37–39], where the authors chose k_0 equal to 1.001 or 1.004. For nominal speed and IM parameters given in Table A.1 in the appendix, values of g_{1-4} are practically equal to zero:

$$\begin{bmatrix} g_1 \\ g_2 \\ g_3 \\ g_4 \end{bmatrix} = \begin{cases} \begin{bmatrix} -5.2207 \cdot 10^{-4} \\ 9.2667 \cdot 10^{-4} \\ -1.6693 \cdot 10^{-6} \\ -2.0582 \cdot 10^{-4} \end{bmatrix} & \text{for } \ k_0 = 1.001, \\ \begin{bmatrix} -2.0883 \cdot 10^{-3} \\ 3.7067 \cdot 10^{-3} \\ -7.3826 \cdot 10^{-6} \\ -8.2328 \cdot 10^{-4} \end{bmatrix} & \text{for } \ k_0 = 1.004. \end{cases} \tag{12}$$

So, both stability and sensitivity to the motor parameter changes of this quasi-open-loop observer were practically the same as for OLO.

2.3. Mathematical models of CS faults

In drive systems with AC motors, using advanced methods for precise control, a crucial component is a CS. For this purpose, Hall-effect transducers, based on the Hall-effect phenomenon, are often employed. According to this phenomenon, when current flows through a conductor placed in a magnetic field perpendicular to the direction of the current flow, a potential difference, known as Hall voltage, arises on opposite sides of the conductor. This voltage depends on the value of the magnetic flux generated by the current flowing through the conductor situated in the magnetic core (see Fig. 1). In line with the Hall effect, this

voltage is proportional to the magnetic flux and, consequently, to the current flowing through the conductor in the core. The primary advantage of Hall effect sensors is their non-contact and non-invasive operation.

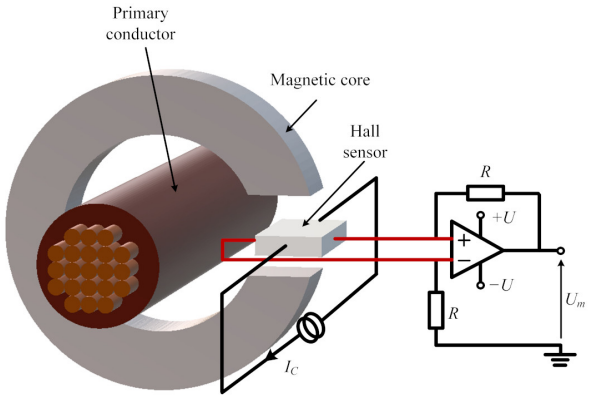

Fig. 1. Measurement of the primary current flowing through the conductor using a Hall sensor

Due to the construction of Hall effect sensors, six typical malfunctions of such systems can be distinguished [15]:

- **Gain error:** It can be caused, among other things, by changes in the output resistor value, damage to electronic components, or incorrect determination of the current-voltage function.
- **Offset:** It may result from a different intersection point of the applied approximation function from the zero point of the current-voltage characteristic.
- **Measurement noise:** It may arise from the accuracy of the measurement transducers, internal interference, or electronic damage. In most cases, measurement noise does not significantly affect the system performance.
- **Saturation:** It is associated with the saturation of the magnetic core.
- **Signal fading** or **total signal loss:** They are related to sensor damage and the interruption of the output signal.

The above-classified faults, along with their mathematical models, are presented in Table 1, while the real current waveform (indexed as r) and the measured current waveform (indexed as m) using a faulty CS are illustrated in Fig. 2.

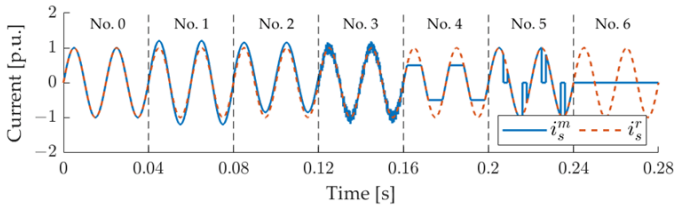

Fig. 2. Waveforms of current for different CS fault types according to Table 1

In ideal conditions, it can be assumed that the current measurement in the drive systems is perfect, as depicted. However, in practice, offsets, gain errors (related to inaccurate scaling of LEM transducers) or measurement noise can often occur. It is important to note, though, that the most critical issues for the drive system are the saturation, the fading, or total loss of the CS signal. In cases where the control structure incorporates protection against exceeding a specified current value, it may not activate when the fault corresponds to no. 4–6 types. In addition, these faults can lead to loss of control over the drive system. Therefore, the presented research primarily focuses on these types of CS faults.

2.4. Direct flux-oriented control

When rewriting the mathematical model of the IM in a synchronously rotating reference frame oriented to the rotor flux vector (as illustrated in Fig. 3), we can control (and stabilize) the rotor flux by using a real component of the stator current vector i_{sx}, and using the imaginary component i_{sy}, we can control

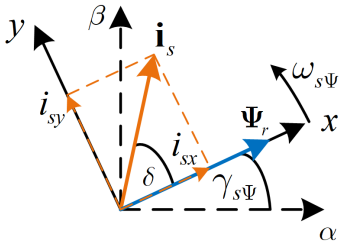

Fig. 3. Idea of DFOC method – vector diagram

Table 1
Fault types with mathematical model

Fault type	Mathematical model	Measurement error
No. 0 No fault	$i_s^m = i_s^r = i_s^r \sin(\omega t)$	$\Delta i_s = i_s^r - i_s^m = 0$
No. 1 Gain error	$i_s^m = n_{\text{gain}} i_s^r$	$\Delta i_s = (1 - n_{\text{gain}}) i_s^r$
No. 2 Offset	$i_s^m = i_s^r + n_{\text{offset}}$	$\Delta i_s = -n_{\text{offset}}$
No. 3 Measurement noise	$i_s^m = i_s^r + n_{\text{noise}}$	$\Delta i_s = -n_{\text{noise}}$
No. 4 Saturation	$i_s^m = \min(n_{\text{sat}}, \lvert i_s^r \rvert) \cdot \text{sign}(i_s^r)$	$\Delta i_s = \max(0, \lvert i_s^r \rvert - n_{\text{sat}}) \cdot \text{sign}(i_s^r)$
No. 5 Signal fading	$i_s^m = [0, i_s^r]$	$\Delta i_s = [i_s^r, 0]$
No. 6 Signal loss	$i_s^m = 0$	$\Delta i_s = i_s^r$

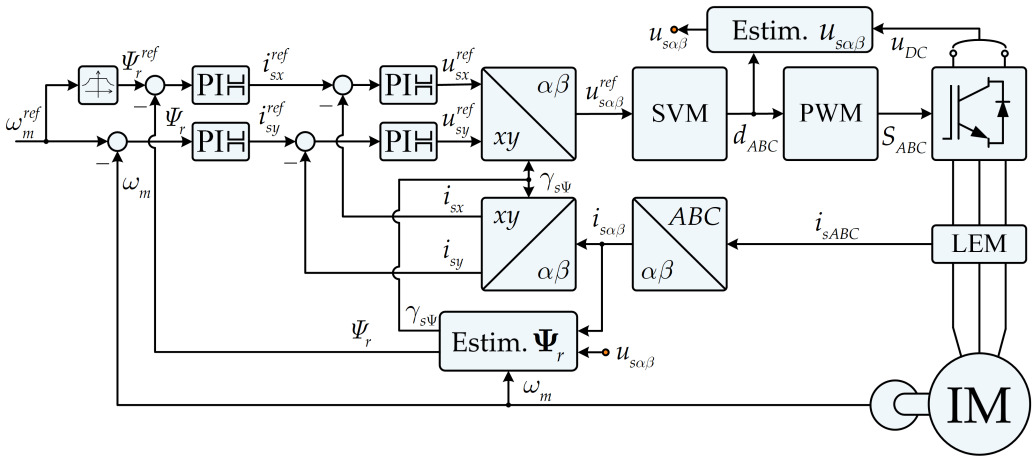

Fig. 4. DFOC scheme

the motor torque, according to the expression:

$$t_{em} = \frac{l_m}{l_r}\Psi_r i_{sy}\,, \tag{13}$$

This approach allows for controlling the IM in a manner analogous to a separately excited DC motor, where the i_{sx} component corresponds to the excitation current, and the i_{sy} component corresponds to the armature current, upon which the electromagnetic torque depends linearly [42].

To implement the DFOC strategy, which is shown in Fig. 4, information about the current value of the rotor flux amplitude and the angle γ_Ψ is required to apply the coordinate transformation $(\alpha-\beta)/(x-y)$. The rotor flux vector can be calculated using any flux estimator method [40]. Its amplitude is given by:

$$\Psi_r = \sqrt{\Psi_{r\alpha}^2 + \Psi_{r\beta}^2}, \tag{14}$$

meanwhile, the angle $\gamma_{s\Psi}$ in this method is calculated using:

$$\gamma_{s\Psi} = \arctan\left(\frac{\Psi_{r\beta}}{\Psi_{r\alpha}}\right). \tag{15}$$

The Park transformation and its inverse are used in this structure:

$$\begin{bmatrix} i_{sx} \\ i_{sy} \end{bmatrix} = \begin{bmatrix} \cos\gamma_{s\Psi} & \sin\gamma_{s\Psi} \\ -\sin\gamma_{s\Psi} & \cos\gamma_{s\Psi} \end{bmatrix} \begin{bmatrix} i_{s\alpha} \\ i_{s\beta} \end{bmatrix}, \\ \begin{bmatrix} i_{s\alpha} \\ i_{s\beta} \end{bmatrix} = \begin{bmatrix} \cos\gamma_{s\Psi} & -\sin\gamma_{s\Psi} \\ \sin\gamma_{s\Psi} & \cos\gamma_{s\Psi} \end{bmatrix} \begin{bmatrix} i_{sx} \\ i_{sy} \end{bmatrix}. \tag{16}$$

2.5. Voltage source inverter dead-time compensation

In a real drive system, it is necessary to compensate for the influence of the dead time of the inverter transistors. It involves an appropriate increase or decrease in the reference voltage value in a given phase, depending on the logical value of the upper switch in that phase. This can be achieved by using the signum function, $\mathrm{sign}(x)$. Compensation can be performed by increasing the absolute values of d_A, d_B, d_C, which constitute the input to the PWM modulator, by a value Δu related to the ratio of dead time T_D to the sampling period T_S [43]:

$$d_p^* = d_p + \Delta u_p\,, \quad p \in \{A,B,C\}, \tag{17}$$

where:

$$\Delta u_p = \frac{T_D}{T_S}\mathrm{sign}\left(i_{sp}\right), \quad p \in \{A,B,C\}. \tag{18}$$

3. METHODS

3.1. Concept of the modified Luenberger observer

The estimation error in LO (9) is defined as the difference between the measured and estimated stator currents in the stationary coordinate system (α–β). However, in CS-FTC systems, when some CS is faulty, it is impossible to properly calculate the value of $\mathbf{e}_i$. It was probably the reason why in [37–39], the authors used such small values of k_0, which makes the $\mathbf{G}$ matrix practically equal to zero (12), and in this case, the estimation error $\mathbf{e}_i$ does not have any impact on LO. It was shown in Section 2.2.

The concept of the MLO involves a different way of calculating the $\mathbf{e}_i$ vector and is directed towards CS-FTC systems. In the first step, the estimated currents expressed in the coordinate system (α–β) are transferred into the phase coordinate system (A–B–C) (according to Clarke transformation [42]:

$$\begin{bmatrix} \hat{i}_{sA} \\ \hat{i}_{sB} \\ \hat{i}_{sC} \end{bmatrix} = \frac{1}{2}\begin{bmatrix} 2\hat{i}_{s\alpha} \\ -\hat{i}_{s\alpha} + \sqrt{3}\hat{i}_{s\beta} \\ -\hat{i}_{s\alpha} - \sqrt{3}\hat{i}_{s\beta} \end{bmatrix}. \tag{19}$$

Due to this measured currents in (9) can be replaced by the corrected currents (upper subscript c):

$$\mathbf{e}_i = \begin{bmatrix} \hat{i}_{s\alpha} - i_{s\alpha}^c & \hat{i}_{s\beta} - i_{s\beta}^c \end{bmatrix}^T, \tag{20}$$

which are calculated depending on the available CS, as follows:

$$\begin{bmatrix} i^c_{s\alpha} & i^c_{s\beta} \end{bmatrix}^T = \begin{cases} \begin{bmatrix} i_{sA} & \frac{\sqrt{3}}{3}\left(i_{sA}+2i_{sB}\right) \end{bmatrix}^T \\ \quad \text{when both CS are healthy,} \\ \begin{bmatrix} -i_{sB}-\hat{i}_{sC} & \frac{\sqrt{3}}{3}\left(\hat{i}_{sA}+2i_{sB}\right) \end{bmatrix}^T \\ \quad \text{when CS in phase } A \text{ is faulty,} \\ \quad \text{CS in phase } B \text{ is healthy,} \\ \begin{bmatrix} i_{sA} & \frac{\sqrt{3}}{3}\left(i_{sA}+2\hat{i}_{sB}\right) \end{bmatrix}^T \\ \quad \text{when CS in phase } A \text{ is healthy,} \\ \quad \text{CS in phase } B \text{ is faulty,} \\ \begin{bmatrix} \hat{i}_{s\alpha} & \hat{i}_{s\beta} \end{bmatrix}^T \\ \quad \text{when both CS are faulty.} \end{cases} \tag{21}$$

As mentioned above, in the existing literature, the authors [37–39] compute the error vector according to the following expression:

$$\mathbf{e}_i = \begin{bmatrix} \hat{i}_{s\alpha} & \hat{i}_{s\beta} \end{bmatrix}^T, \tag{22}$$

which may justify the choice of such a small value of k_0 to make the matrix $\mathbf{G}$ practically negligible (12). However, it should be noted that an extensive analysis conducted in [44] revealed that the selection of the coefficient k_0 values depends on the location of the CS fault. Due to the different methods of calculating the corrected currents (21), the lowest estimation errors of the stator current were obtained with $k_0 = 2.6$ when there was no fault or when the CS fault was in phase A. On the contrary, precise current reproduction was ensured by selecting the coefficient $k_0 = 0.6$ when the fault affected phase B. Therefore, a comparison of the MLO algorithm was performed when the current measurement is not available in phase A (f_A) and phase B (f_B), with the k_0 values chosen based on the analysis presented in [44] ($k_0 = 2.6$ for CS faulty in phase A and $k_0 = 0.6$ for CS faulty in phase B), and with the LO proposed by the aforementioned authors, where the error is calculated according to (9). So, k_0 in this comparison was taken in the range $\{0.6,\ 1.004, 2.6\}$, where 1.004 is the value proposed by the authors of [44] and 0.6 and 2.6 are proposed in the context of this work for the MLO algorithm [44]. The study was carried out assuming that the resistance values of the rotor and the stator are 50% higher, and the main inductance is 25% higher in the IM model compared to the nominal values adopted in the LO model. In Fig. 5, measured and estimated currents using the discussed algorithms are presented during steady state, at nominal speed, and at 75% of the nominal load.

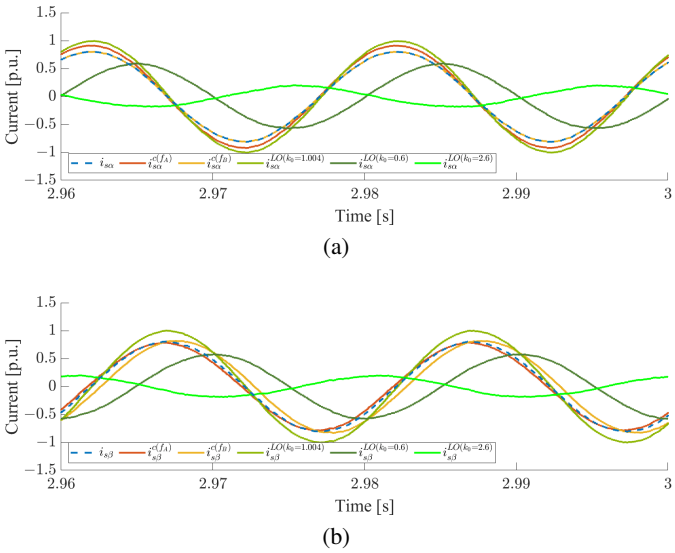

Fig. 5. Waveforms of α (a) and β (b) stator current components f or different estimation methods

For the results presented in Fig. 5, root mean square error (RMSE) values were calculated as follows:

$$\mathrm{RMSE}(i_{sp}) = \sqrt{\frac{\sum_{k=t_1/T_S}^{t_2/T_S+1}\left(i_{sp}(k)-\hat{i}_{sp}(k)\right)^2}{(t_2-t_1)/T_S+1}}, \quad p \in \{\alpha,\ \beta\}, \tag{23}$$

for the selected time range $[t_1,\ t_2]$, where $t_1 = 2.6$ s, $t_2 = 3.0$ s, sampling time, $T_S = 125$ µs.

The obtained values are presented in Table 2.

As can be seen in Table 2, the proposed method yielded much better results. Additionally, it is worth mentioning that the solutions presented in the literature are independent of the number of available CS, due to the use of the formula (21). In the

Table 2
RMSE values of stator current for different estimation methods

Faulty CS	RMSE($i_{s\alpha}$)				RMSE($i_{s\beta}$)			
	$i^c_{s\alpha}$	$i^{LO(k_0=1.004)}_{s\alpha}$	$i^{LO(k_0=0.6)}_{s\alpha}$	$i^{LO(k_0=2.6)}_{s\alpha}$	$i^c_{s\beta}$	$i^{LO(k_0=1.004)}_{s\beta}$	$i^{LO(k_0=0.6)}_{s\beta}$	$i^{LO(k_0=2.6)}_{s\beta}$
No fault	0	0.1368	0.4618	0.6333	0	0.1392	0.4587	0.6317
A	0.0787				0.361			
B	0				0.1181			

case of the proposed method, the corrected currents calculated based on the MLO demonstrate a higher accuracy.

As demonstrated by the analysis in [44], the best results in the estimation of phase currents that were not available for measurement were achieved for the following values of the coefficient k_0:

- $k_0 = 2.6$ for healthy CS or faulty CS only in phase A,
- $k_0 = 0.6$ for faulty CS only in phase B.

However, to estimate the currents for the detection system (estimation of the phase current for the available CS in a given phase), the best results were obtained for $k_0 = 2.6$. Therefore, in the developed CS-FTC structure, two MLO algorithms are proposed – one with a constant value of k_0 for estimating currents used for the detection system, and the other one, with an adaptive value of k_0 depending on the available CS, used for calculating corrected currents utilized in computing the error vector $\mathbf{e}_i$ and in the control structure, when one of the CS is damaged).

3.2. Current sensor fault detection

A significant issue related to detectors based on mathematical models of some signals is their dependence on IM parameters. However, as shown in Fig. 5, the proposed MLO is less sensitive to changes in IM parameters than others presented in the literature [44].

To detect faults in CS, a simple algorithm was developed. In this case, the first step is to calculate estimated phase currents, according to (19). Next, a square of the difference between the estimated and measured stator current should be calculated as:

$$\varepsilon_p(k) = \left(i_{sp}(k) - \hat{i}_{sp}(k)\right)^2, \quad p \in \{A, B\}. \tag{24}$$

If the ε coefficient is larger than the assumed permissible threshold, then a fault will be detected. However, to reduce the number of false detections, it was assumed that the value of ε should exceed the threshold for two consecutive samples. Additionally, the CS-FD system maintains the information about the fault after detection. The entire process is presented in Fig. 6.

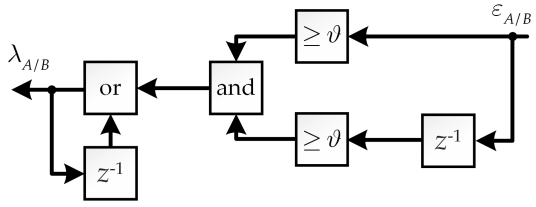

Fig. 6. A scheme of the proposed CS-FD system

Coefficient λ in a given phase, presented in Fig. 6, is equal to 0 for healthy CS and equal to 1 for faulty CS. To accurately determine the location of the CS fault, the resulting value of $\lambda$is calculated as follows:

$$\lambda = \lambda_A + 2\lambda_B + 1. \tag{25}$$

In this regard, the fault location is determined as follows:

- $\lambda = 1$ – both CS are healthy,
- $\lambda = 2$ – CS in phase A is faulty,
- $\lambda = 3$ – CS in phase B is faulty,
- $\lambda = 4$ – both CS are defective.

To develop a precise detection system, it is necessary to obtain the maximum value of $\varepsilon_{A/B}$. For example, for gain fault in A-phase CS, this maximum value can be calculated as follows:

$$\max\left(\varepsilon_A(k)\right) = \left(n_{\text{gain}} - 1\right)^2 \hat{i}^2_{sA}(k). \tag{26}$$

Transforming the above equation yields:

$$n_{\text{gain}} = 1 \pm \frac{\max\left(\varepsilon_A(k)\right)}{\left|\hat{i}_{sA}(k)\right|}. \tag{27}$$

Assuming that the maximum gain error is equal to $\pm\delta \cdot 100\%$:

$$\max\left(\varepsilon_A(k)\right) = \delta^2 \hat{i}^2_{sA}(k). \tag{28}$$

As can be seen, in this case, the maximum gain error is dependent on the stator current value. It should be highlighted that the gain error is the biggest for the maximum value of the stator current. Due to this, the maximum permissible threshold value is dependent on the stator current amplitude in the following way:

$$\vartheta = \delta^2 \hat{i}^2_s. \tag{29}$$

For an offset error in phase A, the maximum error value ε value is:

$$\max\left(\varepsilon_A(k)\right) = n^2_{\text{offset}}. \tag{30}$$

As can be seen, the maximum permissible value of offset error is also $\pm\delta \cdot 100\%$:

$$n_{\text{offset}} = \delta \hat{i}_s. \tag{31}$$

During start-up, the value of the stator current at time $t = 0$ is equal to zero. To avoid false FD during startup, a minimum value of the coefficient was assumed, dependent on the vector length of corrected current and the amplitude of the current during no-load operation, i_{s0}, (in this research, the approximate value of this current is equal to 0.4):

$$\vartheta = \delta^2 \cdot \max\left(i^c_s;\, i_{s0}\right). \tag{32}$$

It was observed that, at higher speeds, the error between the measured and estimated currents was greater. Therefore, it was decided to further modify the threshold ϑ, depending on the angular speed, according to:

$$\vartheta = \delta^2 \cdot \max\left(i^c_s;\, i_{s0}\right) \cdot f(\omega_m), \tag{33}$$

where:

$$f(\omega_m) = \begin{cases} (\alpha_\omega - 1)\dfrac{|\omega_m|}{\omega_{mN}} + \alpha_\omega & \text{for } t \geq t_\omega, \\ 1 & \text{for } t < t_\omega \end{cases}, \tag{34}$$

and $\delta \cdot 100\% = 20\%$; $\alpha_\omega = 0.3$; $t_\omega = 0.3$ s.

According to the above equation, the coefficient ϑ is linearly dependent on the motor speed, such that at its nominal value, the

value of the coefficient (33) is equal to (32). However, for very small speeds, the coefficient (33) reaches 30% of the value (32). Additionally, a minimum time of 0.3 seconds was determined to avoid false detections in the initial startup time (0.3 s is approximately twice the time required for the rotor flux to stabilize after the startup). The results of the detection have been presented in the section on experimental verification.

3.3. Current sensor fault compensation

The CS-FC is also based on the currents estimated by MLO, but as shown above in Section 2.2, in this case, the value of the coefficient k_0 is dependent on the available CS (likewise from the value of the coefficient λ (25)), as follows:

$$k_0 = f(\lambda) = \begin{cases} 2.6 & \text{for } \lambda = 2, \\ 0.6 & \text{for } \lambda = 3, \\ 1 & \text{for } \lambda = 1 \vee \lambda = 4. \end{cases} \tag{35}$$

When λ is equal to 1, it means that the corrected currents are equal to the measured currents, and in such a situation, no correction is required. However, when λ is equal to 4, it indicates a lack of any information about the measured currents, making error correction impossible. In both cases, k_0 is equal to 1, reducing this MLO to a simple simulator. It is important to emphasize that the occurrence of faults in two CSs is rare, and knowledge of at least one signal from CS allows for a significant improvement in the quality of CS-FTC system operation.

3.4. Current sensor fault tolerant control

In summary, for fault detection, MLO_D (D index – detection) is used with a constant coefficient value k_0 equal to 2.6. Meanwhile, for calculating corrected currents (21), utilized in the control structure and to determine the estimation error of the observers $\mathbf{e}_i$ (20), the MLO_C (C index – compensation) is used with an adaptive k_0 according to (35). The overall CS-FTC strategy is shown in Fig. 7.

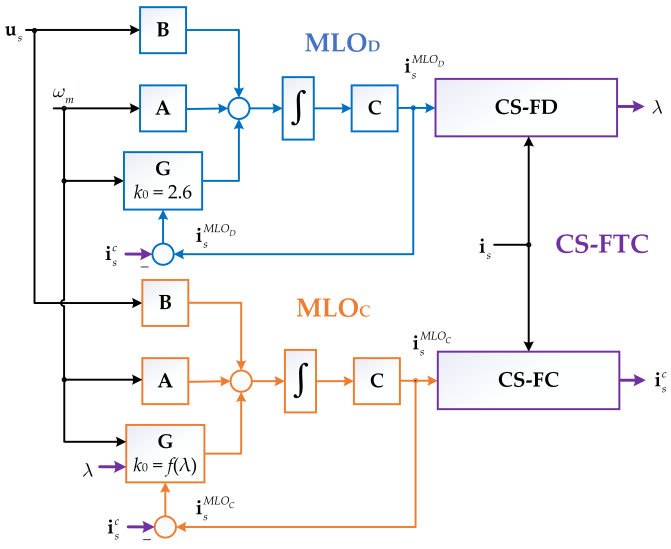

Fig. 7. A scheme of the proposed CS-FTC system

4. EXPERIMENTAL VERIFICATION

4.1. Laboratory set-up description

All experiments have been conducted using algorithms developed in the MATLAB/Simulink. Calculations were realized with a step equal to the PWM cycle: $T_S = 125$ µs. Measurement results were collected and displayed through the ControlDesk environment. The tested 1.1 kW (see parameters in Table A.1) was loaded by a second motor of 1.5 kW motor. An optical fiber card was utilized for transistor control. The laboratory setup is presented in Fig. 8.

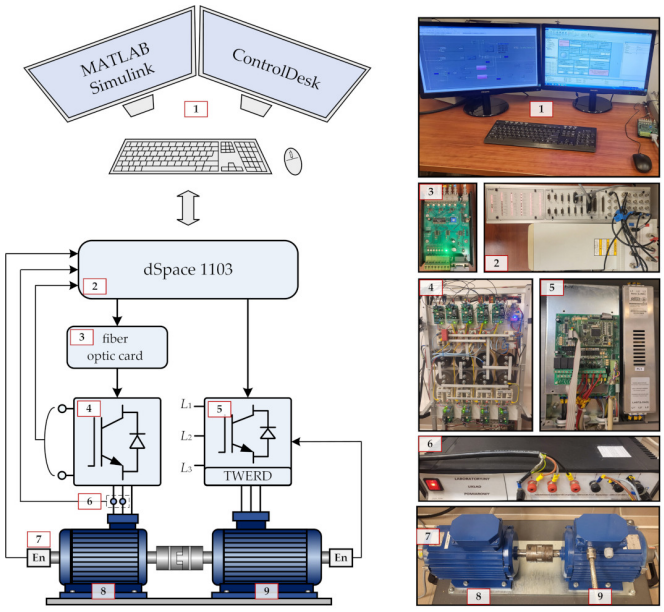

Fig. 8. Diagram of the laboratory set-up

The elements of the set-up are as follows: 1 – PC-class computer, 2 – dSpace 1103 with connection panel, 3 – fiber optic card, 4 – frequency converter for motor control, 5 – frequency converter for load torque control, 6 – incremental encoder, 7 – LEM type transducers, 8 – 3-phase IM (controlled), 9 – 3-phase IM (load).

4.2. Analysis of CS fault detector pre-fault operation

First, the behavior of the CS-FD was examined assuming that the CS in the discussed phase is healthy. The purpose was to investigate whether the CS-FD does not generate false signals. Studies were conducted for two load torque values 25% and 75% of the rated value, along with a wide range of angular velocity changes: 100%, 75%, 50%, 25%, 10%, 5%, 3%, 1% of the rated value (see Fig. 9). Additionally, all tests were performed in both

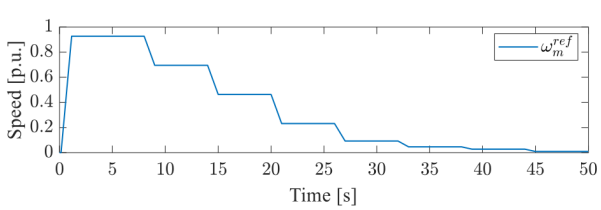

Fig. 9. Waveforms of the reference speed

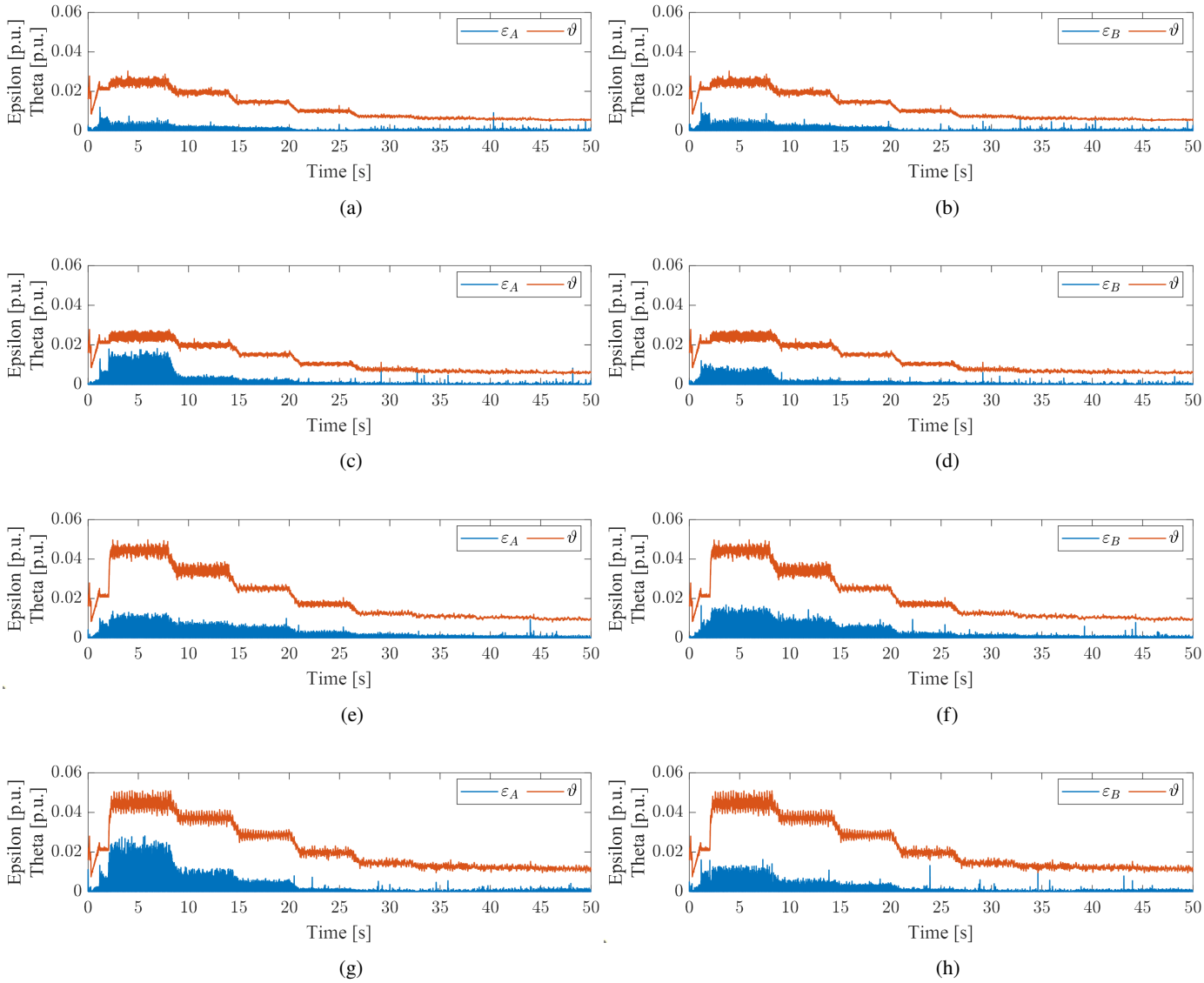

Fig. 10. Waveforms epsilon and theta coefficient in phase A (a, c, e, g) and B (b, d, f, h) for motoring (a, b, e, f) and regenerating (c, d, g, h) operations, 25% of the rated load (a, b, c, d) and 75% of the rated load (e, f, g, h)

motoring and regenerating modes. Figures 10a–d present the results for 25% of the rated load, and Figs. 10e–h for 75%.

As observed in Figs. 10 and 11, the threshold value changes adaptively depending on the load torque and angular velocity. For 75% of the rated load, the square of the difference between the measured and estimated current is greater than for 25% of the load. Consequently, the threshold coefficient decreases with a reduction in the estimation error, even to a value of 0.005 [p.u.]. The dependency of the threshold ϑ on the operating point of the drive enables an increase in the detector sensitivity to the appearance of potential faults. Despite the occurrence of individual error impulses exceeding the threshold value, no identical error was obtained for two consecutive samples in any analyzed waveform. This means that the system based on the adaptive threshold coefficient (33) and the adopted detection algorithm (Fig. 7) did not make a single incorrect detection throughout the analysis.

4.3. Analysis of the CS-FTC system at variable speeds

For the analyzed case, the faults occurred in dynamic states and were as follows:

- Measurement offset of 0.3 in phase A at $t = 6.3$ s and gain error of 1.3 in phase B at $t = 12.8$ s (Figs. 11a, c, e, g, i, k).
- Signal saturation of 0.5 in phase B at $t = 9.2$ s and total loss of signal in phase A at $t = 18.4$ s (Figs. 11b, d, f, h, j, l).

In the event of gain and offset faults, as well as saturation and signal loss, it is noticeable that the motor speed is effectively controlled (Figs. 11a, b). The rotor flux and electromagnetic torque waveforms (Figs. 11c–f) practically deviate insignificantly from the waveforms during normal system operation. All four faults (measurement offset in phase A at $t = 6.3$ s and gain error in phase B at $t = 12.8$ s in the first case, as well as saturation in phase B at $t = 9.2$ s and the total loss of signal in phase A at $t = 18.4$ s) were detected (Figs. 11g, h) and appropriately compensated (Figs. 11k, l). In Figs. 11i, j, the re-

markably high precision of reconstruction of the phase currents used in the detector can be observed. Additionally, it should be noted that despite the failure of all CSs available in the drive system, the proposed strategy allows for the continued vector control of the drive without the need to switch to scalar control.

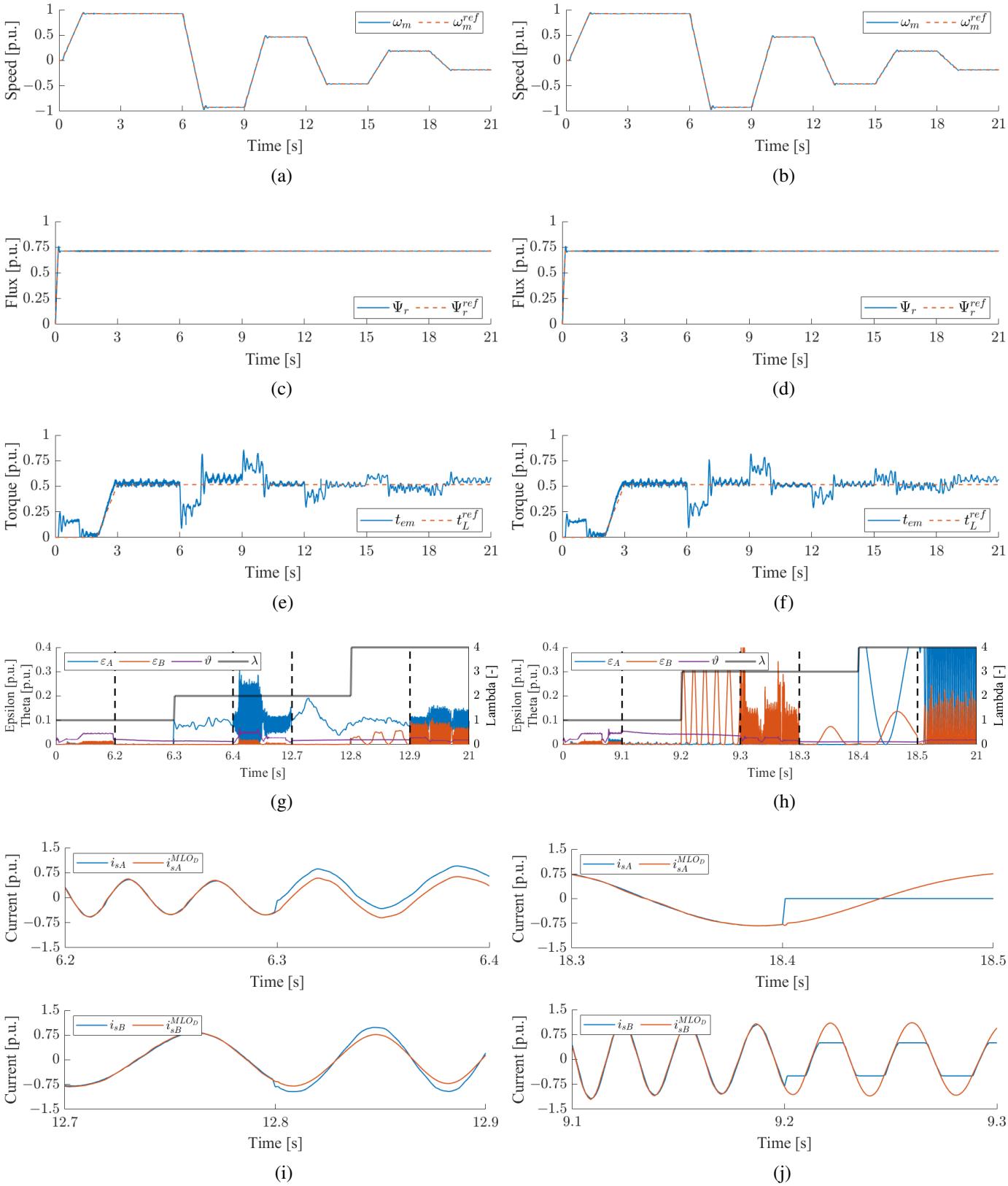

Fig. 11

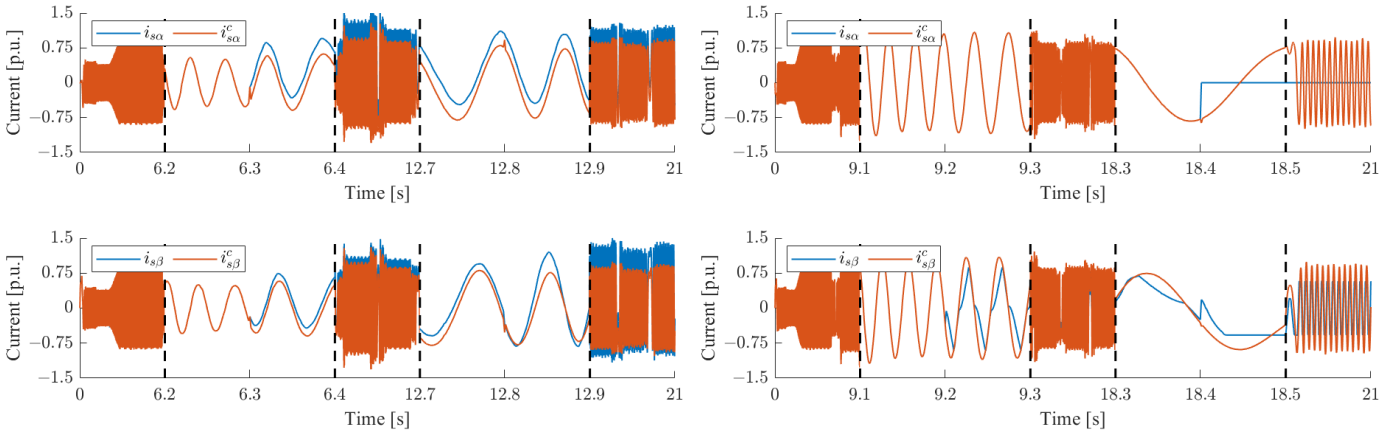

(k) (l)

Fig. 11. Waveforms of state variables: speed (a, b), rotor flux (c, d), torque (e, f), coefficients (g, h), and currents used in the detector (i, j), corrected currents; gain and offset (a, c, e, g, i, k), saturation and total signal loss (b, d, f, h, j, l)

4.4. Analysis of the CS-FTC system at variable loads

For the analyzed case, the faults occurred in dynamic states and were as follows:

- Measurement offset of −0.3 in phase B at $t = 9.2$ s and gain error of 1.3 in phase A at $t = 18.7$ s (Figs. 12a, c, e, g, i, k).
- Signal saturation of 0.5 in phase A at $t = 2.6$ s and total signal loss in phase B at $t = 6.5$ s (Figs. 12b, d, f, h, j, l).

In this scenario as well, regardless of the order and type of faults, the CS-FTC system demonstrated high effectiveness, as evident in the angular velocity, rotor flux, and electromagnetic torque waveforms (Figs. 12a–f). In this situation, the faults were promptly detected (Figs. 12g, h) and compensated (Figs. 12k, l). The high quality is further attested by the precision in reproducing the currents used in the detector (Figs. 12i, j).

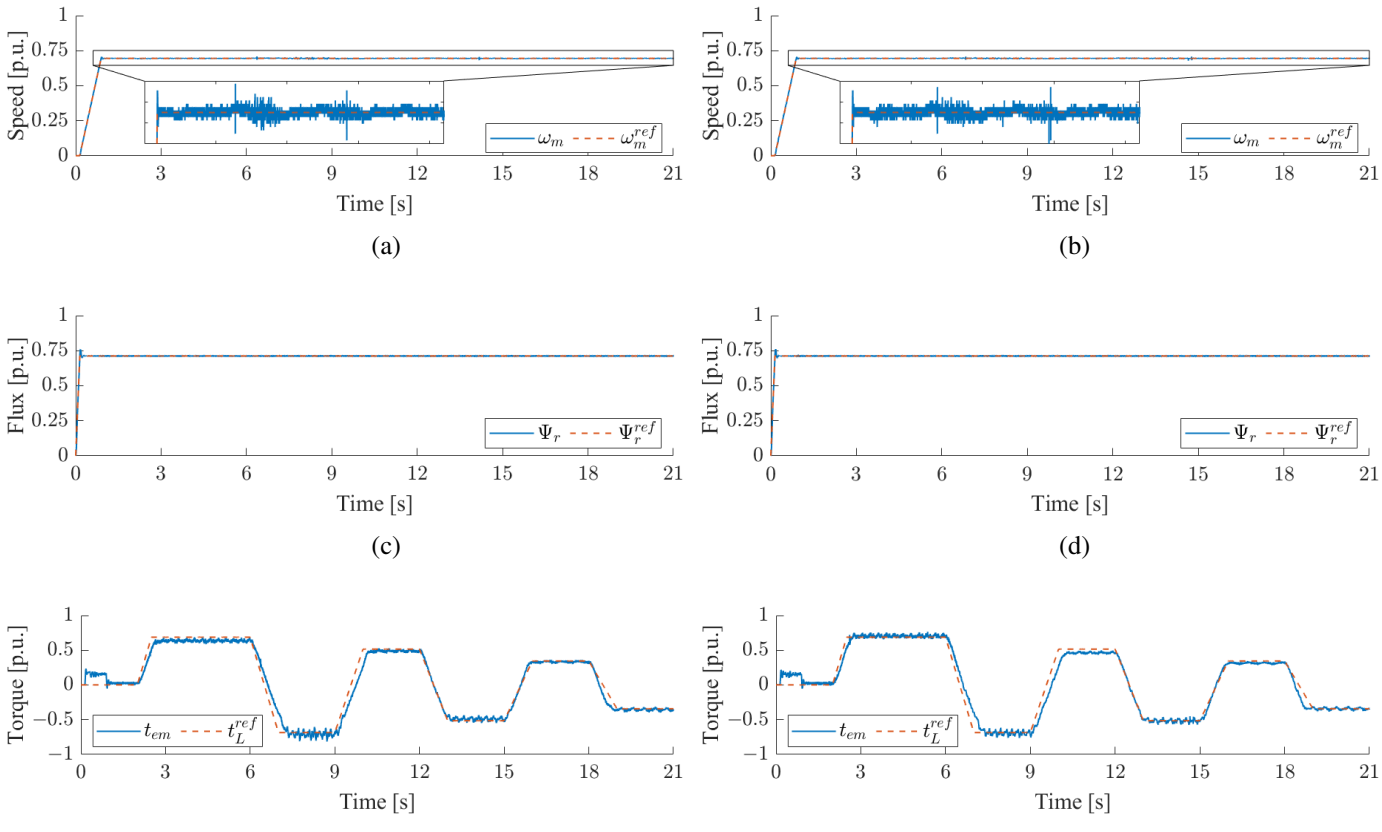

(a) (b)

(c) (d)

(e) (f)

Fig. 12

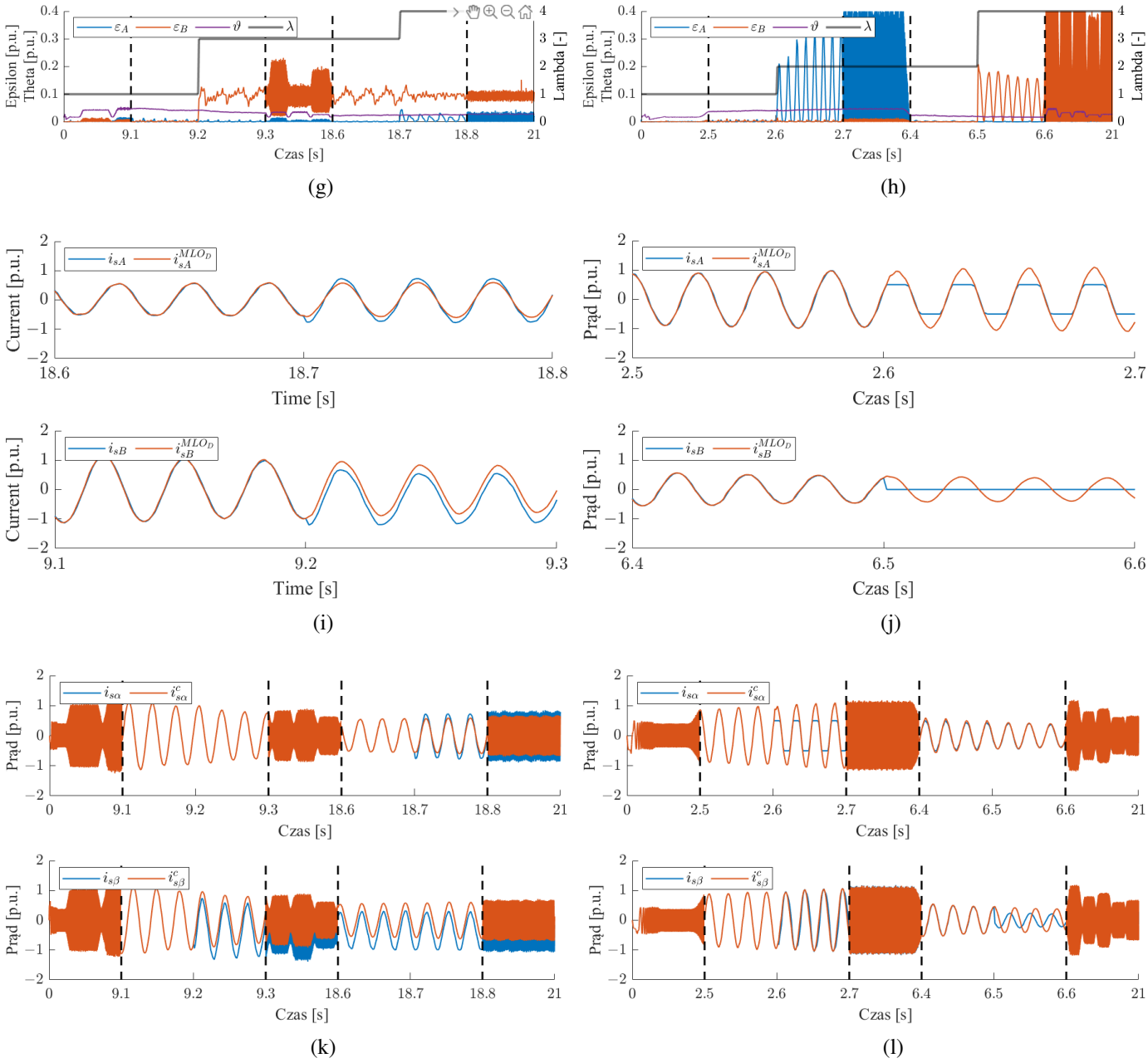

Fig. 12. Waveforms of state variables: speed (a, b), rotor flux (c, d), torque (e, f), coefficients (g, h), and currents used in the detector (i, j), corrected currents; gain and offset (a, c, e, g, i, k), saturation and total signal loss (b, d, f, h, j, l)

5. CONCLUSIONS

The presented article introduces a comprehensive CS-FTC structure. The proposed fault detector with an adaptive threshold allowed precise fault detection, regardless of the type of fault (offset, gain error, saturation, or loss of signal), as demonstrated by experimental studies. Furthermore, it should be noted that CS faults occurred both during motor and generator operation, as well as in dynamic states, and were properly detected.

Additionally, it should be emphasized that, since the algorithm is based on two MLOs, high-quality currents are used in the detector, and corrected currents are achieved. This enables the development of a CS-FTC system characterized by very high operational quality. In each case analyzed, the angular velocity was fully controlled. Moreover, no difference in the performance of the structure was observed, with one functioning CS or without any CSs. The proposed solution is cost-effective and can be applied to safety-critical IM drives with vector control such as electric vehicles, where the field-oriented control of electromagnetic torque and speed should also be preserved after CS fault.

ACKNOWLEDGEMENTS

This work was supported in parts by the National Science Centre Poland under Grant 2021/41/B/ST7/02971.

APPENDIX

Table A.1
Rated parameters of IM

Symbol	[ph.u.]	[p.u.]
Rated phase voltage, U_N	230 V	0.707
Rated phase current, I_N	2.5 A	0.707
Rated power, P_N	1.1 kW	0.638
Rated speed, n_N	1390 rpm	0.927
Rated torque, T_{eN}	7.56 Nm	0.688
Number of pole pairs, p_b	2	–
Rotor winding resistance, R_r	4.968 Ω	0.0540
Stator winding resistance, R_s	5.114 Ω	0.0556
Rotor leakage inductance, $L_{\sigma r}$	31.6 mH	0.1079
Stator leakage inductance, $L_{\sigma s}$	31.6 mH	0.1079
Main inductance, L_m	541.7 mH	1.8498
Rated rotor flux, Ψ_{rN}	0.7441 Wb	0.7187
Mechanical time constant, T_M	0.25 s	–

REFERENCES

[1] Z. Gao, C. Cecati, and S.X. Ding, "A Survey of Fault Diagnosis and Fault-Tolerant Techniques—Part I: Fault Diagnosis with Model-Based and Signal-Based Approaches," *IEEE Trans. Ind.*, vol. 62, no. 6, pp. 3757–3767, June 2015.

[2] Z. Gao, C. Cecati and S.X. Ding, "A Survey of Fault Diagnosis and Fault-Tolerant Techniques – Part II: Fault Diagnosis with Knowledge-Based and Hybrid/Active Approaches," *IEEE Trans. Ind. Electr.*, vol. 62, no. 6, pp. 3768–3774, June 2015.

[3] M.A. Djeziri, R. Merzouki, B.O. Bouamama, and M. Ouladsine, "Fault Diagnosis and Fault-Tolerant Control of an Electric Vehicle Overactuated," *IEEE Trans. Vehicular Tech.*, vol. 62, no. 3, pp. 986–994, March 2013.

[4] T. Orlowska-Kowalska *et al.*, "Fault diagnosis and fault-tolerant control of PMSM drives – state of the art and future challenges", *IEEE Access*, vol. 10, pp. 59979–60024, June 2022.

[5] M. Santosh Kumar, V.B. Borghate, R.R. Karasani, S. Sabyasachi and H.M. Suryawanshi, "A fault-tolerant modular multilevel inverter topology", *Int. J. Circuit Theory Appl.*, vol. 46, no. 5, pp. 1028–1043, 2018.

[6] J. Li, B. Du, T. Zhao, S. Wu, and S. Cui, "Current Sensor Fault-Tolerant Control for Five-Phase PMSM Drives Based on Third-Harmonic Space," *IEEE Trans. Ind. Electr.*, vol. 69, no. 10, pp. 9827–9837, Oct. 2022.

[7] M. Dybkowski, K. Klimkowski, "Stator current sensor fault detection and isolation for vector controlled induction motor drive," in *Proc. IEEE Int. Electronics and Motion Control Conf. (PEMC)*, Varna, Bulgaria, 25–28 Sept. 2016; pp. 1097–1102.

[8] M. Korzonek, G. Tarchala, and T. Orlowska-Kowalska, "A review on MRAS-type speed estimators for reliable and efficient induction motor drives," *ISA Trans.*, vol. 93, pp. 1–13, 2019.

[9] T. Orlowska-Kowalska, M. Korzonek, and G. Tarchala, "Stability Improvement Methods of the Adaptive Full-Order Observer for Sensorless Induction Motor Drive—Comparative Study," *IEEE Trans. Ind. Inf.*, vol. 15, no. 11, pp. 6114–6126, Nov. 2019.

[10] M. Morawiec, P. Kroplewski, Nonadaptive estimation of the rotor speed in an adaptive full order observer of induction machine, *Bull. Pol. Acad. Sci. Tech. Sci.*, vol. 68, no. 5, pp. 973–981, 2020.

[11] C. Chakraborty and V. Verma, "Speed and Current Sensor Fault Detection and Isolation Technique for Induction Motor Drive Using Axes Transformation," *IEEE Trans. Ind. Electr.*, vol. 62, no. 3, pp. 1943–1954, March 2015.

[12] M. Kuchar, P. Palacky, P. Simonik, and J. Strossa, "Self-tuning observer for sensor fault-tolerant control of induction motor drive", *Energies*, vol. 14, no. 9, pp. 2564, Apr. 2021.

[13] T.A. Najafabadi, F.R. Salmasi and P. Jabehdar-Maralani, "Detection and Isolation of Speed-, DC-Link Voltage-, and CurrentSensor Faults Based on an Adaptive Observer in Induction-Motor Drives," *IEEE Trans. Ind. Electr.*, vol. 58, no. 5, pp. 1662–1672, May 2011.

[14] X. Shi and M. Krishnamurthy, "Survivable Operation of Induction Machine Drives with Smooth Transition Strategy for EV Applications," *IEEE Journal of Emerg. Sel. Topics in Power Electr.*, vol. 2, no. 3, pp. 609–617, Sept. 2014.

[15] K.-S. Lee and J.-S. Ryu, "Instrument fault detection and compensation scheme for direct torque controlled induction motor drives," *IEE Proc. Control Theory and Applications*, vol. 150, no. 4, pp. 376–382, Jul. 2003.

[16] F. Aguilera, P.M. de la Barrera, C.H. De Angelo, and D.R. Espinoza Trejo, "Current-sensor fault detection and isolation for induction-motor drives using a geometric approach," *Control Eng. Practice*, vol. 53, pp. 35–46, 2016.

[17] D.W. Chung and S.K. Sul, "Analysis and compensation of current measurement error in vector-controlled AC motor drives," *IEEE Trans. Ind. Appl.*, vol. 34, no. 2, pp. 340–345, 1998.

[18] K. Rothenhagen and F.W. Fuchs, "Model-based fault detection of gain and offset faults in doubly fed induction generators," in *Proc. 2009 IEEE Int. Symp. Diagn. Electric Machines, Power Electronics and Drives, (SDEMPED)*, 2009.

[19] F.R. Salmasi, "A Self-Healing Induction Motor Drive With Model Free Sensor Tampering and Sensor Fault Detection, Isolation, and Compensation," *IEEE Trans. Ind. Electr.*, vol. 64, no. 8, pp. 6105–6115, 2017.

[20] T.C. Green and B.W. Williams, "Derivation of Motor Line-Current Waveforms from the DC-Link Current of an Inverter," *IEE Proc. B-Electric Power Appl.*, vol. 136, no. 4, pp. 196–204, 1989.

[21] W.C. Lee, D.S. Hyun, and T.K. Lee, "A novel control method for three-phase PWM rectifiers using a single current sensor," *IEEE Trans. Power Electron.*, vol. 15, no. 5, pp. 861–870, 2000.

[22] B. Metidji, N. Taib, L. Baghli, T. Rekioua, and S. Bacha, "Low-cost direct torque control algorithm for induction motor without AC phase current sensors," *IEEE Trans. Power Electron*, vol. 27, no. 9, pp. 4132–4139, 2012.

[23] J.I. Ha, "Current prediction in vector-controlled PWM inverters using single DC-link current sensor," *IEEE Trans. Ind. Electron.*, vol. 57, no. 2, pp. 716–726, 2010.

[24] H. Kim and T.M. Jahns, "Current control for AC motor drives using a single DC-link current sensor and measurement voltage vectors," *IEEE Trans. Ind. Appl.*, vol. 42, no. 6, pp. 1539–1547, 2006.

[25] W. Wang, M. Cheng, Z. Wang, and B. Zhang, "Fast switching direct torque control using a single DC-link current sensor," *J. Power Electron.*, vol. 12, no. 6, pp. 895–903, 2012.

[26] Y. Xu, H. Yan, J. Zou, B. Wang, and Y. Li, "Zero Voltage Vector Sampling Method for PMSM Three-Phase Current Reconstruction Using Single Current Sensor," *IEEE Trans. Power Electron.*, vol. 32, no. 5, pp. 3797–3807, 2017.

[27] W. Wang, Y. Feng, Y. Shi, M. Cheng, W. Hua, and Z. Wang, "Fault-Tolerant Control of Primary Permanent-Magnet Linear Motors With Single Phase Current Sensor for Subway Applications," *IEEE Trans. Power Electron.*, vol. 34, no. 11, pp. 10546–10556, Nov. 2019.

[28] Y. Yu, Y. Zhao, B. Wang, X. Huang, and D. Xu, "Current Sensor Fault Diagnosis and Tolerant Control for VSI-Based Induction Motor Drives," *IEEE Trans. Power Electron.*, vol. 33, no. 5, pp. 4238–4248, May 2018.

[29] F.R. Salmasi and T.A. Najafabadi, "An Adaptive Observer with Online Rotor and Stator Resistance Estimation for Induction Motors with One Phase Current Sensor," *IEEE Trans. Energy Conv.*, vol. 26, no. 3, pp. 959–966, Sept. 2011.

[30] Y. Chen, D. Xie, Y. Zuo, Y. Chang, and X. Ge, "Current Sensor Fault-Tolerant Control for Induction Motor with SpeedSensorless Based on SMO and SEPLL," in *Proc. 2021 24th Int. Conf. on Electrical Machines and Systems (ICEMS)*, 2021, pp. 1988–1992.

[31] Y. Zuo, X. Ge, Y. Chang, Y. Chen, D. Xie, H. Wang, and A.T. Woldegiorgis, "Current Sensor Fault-Tolerant Control for Speed-Sensorless Induction Motor Drives Based on the SEPLL Current Reconstruction Scheme," *IEEE Trans. Ind. Appl.*, vol. 59, no. 1, pp. 845–856, Jan.-Feb. 2023.

[32] M. Manohar and S. Das, "Current Sensor Fault-Tolerant Control for Direct Torque Control of Induction Motor Drive Using Flux-Linkage Observer," *IEEE Trans. Ind. Inform.*, vol. 13, no. 6, pp. 2824–2833, Dec. 2017.

[33] M. Adamczyk and T. Orlowska-Kowalska, "Virtual current sensor in the fault-tolerant field-oriented control structure of an induction motor drive," *Sensors*, vol. 19, no. 22, p. 4979, 2019, doi: 10.3390/s19224979.

[34] M. Adamczyk and T. Orlowska-Kowalska, "Postfault Direct Field-Oriented Control of Induction Motor Drive Using Adaptive Virtual Current Sensor," *IEEE Trans. Ind. Electron.*, vol. 69, no. 4, pp. 3418–3427, April 2022.

[35] M. Adamczyk and T. Orlowska-Kowalska, "Influence of the Stator Current Reconstruction Method on Direct Torque Control of Induction Motor Drive in Current Sensor Postfault Operation," *Bull. Pol. Acad. Sci. Tech. Sci.*, vol. 70, no. 1, p. e140099, 2022, doi: 10.24425/bpasts.2022.140099.

[36] L.E. Venghi, F. Aguilera, P.M. De La Barrera and C.H. De Angelo,"Current-sensors fault tolerant control system for electric drives: experimental validation," in *Proc. 2021 XIX Workshop on Inf. Processing and Control (RPIC)*, 2021, pp. 1–6.

[37] Y. Azzoug *et al.*, "An Active Fault-Tolerant Control Strategy for Current Sensors Failure for Induction Motor Drives Using a Single Observer for Currents Estimation and Axes Transformation," *Eur. J. Electr. Eng.*, vol. 23, no. 6, pp. 467–474, Dec. 2021.

[38] Y. Azzoug, M. Sahraoui, R. Pusca, T. Ameid, R. Romary, and A.J.M. Cardoso, "High-performance vector control without AC phase current sensors for induction motor drives: Simulation and real-time implementation," *ISA Trans.*, vol. 109, pp. 295–306, Mar. 2021.

[39] Y. Azzoug, M. Sahraoui, R. Pusca, T. Ameid, R. Romary, and A.J. Marques Cardoso, "Current sensors fault detection and tolerant control strategy for three-phase induction motor drives," *Electr. Eng.*, vol. 103, no. 2, pp. 881–898, Apr. 2021.

[40] T. Orlowska-Kowalska, *Sensoless Induction Motor Drives*, Wroclaw, Poland: Wroclaw University of Technology Press, 2003.

[41] D. Luenberger, "An introduction to observers," *IEEE Trans. Aut. Contr.*, vol. 16, no. 6, pp. 596–602, December 1971.

[42] M.P Kazmierkowski, R. Krishnan, and F. Blaabjerg, *Control in Power Electronics – Selected Problems*. USA, Academic Press, 2002.

[43] N. Urasaki, T. Senjyu, K. Uezato, and T. Funabashi, "On-line dead-time compensation method for permanent magnet synchronous motor drive," *2002 IEEE Int. Conf. Ind. Tech., ICIT'02*, Bankok, Thailand, 2002, pp. 268–273.

[44] M. Adamczyk and T. Orlowska-Kowalska, "Influence of Parameter Uncertainty to Stator Current Reconstruction Using Modified Luenberger Observer for Current Sensor Fault-Tolerant Induction Motor Drive," *Sensors*, vol. 22, no. 24, p. 9813, 2022.